

**DEVELOPMENT OF AN AUTO-FOCUSING
FLUID LENS SYSTEM**

SORAN JALAL ABDULLAH

UNIVERSITI SAINS MALAYSIA

2009

DEVELOPMENT OF AN AUTO-FOCUSING FLUID LENS SYSTEM

by

SORAN JALAL ABDULLAH

**Thesis submitted in fulfillment of the requirements
for the degree of
Master of Science**

April 2009

ACKNOWLEDGEMENT

All Praise be to *Allah*, the *Bestower* of all Goodness, for bestowing His grace and mercy upon us in this Life and for granting us the opportunity to seek his forgiveness for the Hereafter. Truly, the more we learn, the more we realize the greatness of the *Creator*.

I would like to express my deepest appreciation and gratitude to my Supervisor, Assoc. Prof. Dr. Mani Maran Ratnam, for his courteous treatment, support and guidance throughout the project execution. Indeed, he showed much concern for the welfare and wellbeing of the student. I also would like to extend my thanks and appreciation to my co-supervisor Assoc. Prof. Dr. Zahurin Samad for his willingness and readiness to help whenever I approached him. I thank the program leader of NOR lab Prof. Dr. Kamarulazizi Ibrahim and Dr. Magdi along with the staff for their support during the diaphragm fabrication.

I dedicate this project to my wonderful father, Prof. Dr. Jalal Abdullah Aziz, to whom I am greatly and deeply indebted for life. I may only say to him “Jazakallalhu khairal jaza’ in Dunia and Akhirah”, i.e., May only *Allah* reward you with the best of the reward in this Life and in the Hereafter.

Many thanks to the technical staff: Br. Ashamuddin, Br. Zaimi, Encik Hamid and Encik Kamarulddin for their help during the hardware setup preparation. My best wishes go to all those who helped whenever I needed.

Finally, I end as I started with the Praise of *Allah* who has given us the gift of mind to ponder upon His creation.

TABLE OF CONTENTS

	Page
Acknowledgement	ii
Table of Contents	iii
List of Tables	viii
List of Figures	ix
List of Abbreviations	xxii
Abstrak	xxiii
Abstract	xxiv
CHAPTER 1 – INTRODUCTION	
1.1 Research Background	1
1.2 Problem Statement	3
1.3 Research Objective	4
1.4 Research Scope	5
1.5 Research Methodology	6
1.6 Thesis Organization	7
CHAPTER 2 – LITERATURE REVIEW	
2.1 Introduction	9
2.2 Liquid Crystal Lens	9
2.3 Electrowetting-Based Lens	11
2.4 Hydrogel-Based Lens	13
2.5 Diaphragm Fluid Lens	16
2.5.1 Lens Theorization, Fabrication, Characterization and Testing	17

2.5.2	Actuation Methods and Control	24
2.6	Summary	29
CHAPTER 3 – FINITE ELEMENT ANALYSIS OF FLUID LENS		
DIAPHRAGM		
3.1	Introduction	30
3.2	Type and Method Selection for the Finite Element Analysis	32
3.2.1	Background	32
3.2.2	Procedure of Type and Method Selection	35
3.1.2(a)	Diaphragm Material Properties	39
3.1.2(b)	Load and Boundary Conditions	40
3.2.3	Outcome of the Type and Method Selection	41
3.3	Commercial Software Validation	48
3.3.1	Comparison with Published Work	49
3.3.2	Comparison Results	50
3.4	Determination of Fluid Lens Design Parameters	51
3.4.1	FEA Simulation of Various Diaphragms	51
3.4.2	Simulation Results for the Diaphragm Models	53
3.5	Analysis of Diaphragm Shape	56
3.5.1	Method of Diaphragm Shape Analysis	57
3.5.1(a)	Finding the Approximate Circular Fit	58
3.5.1(b)	Identification of Parameters of Interest	60
3.5.1(c)	Diaphragm Thickness Deviation	61
3.5.2	Results of the Diaphragm Shape Analysis	61
3.6	Summary	67

CHAPTER 4 – OPTICAL MATHEMATICAL MODELING

4.1	Introduction	68
4.2	Model Derivation	69
4.2.1	Model for Single-Refraction Lens	69
4.2.2	Double-Refraction (Plano-Convex) Lens	77
4.3	Summary of the Optical Mathematical Modeling	81

CHAPTER 5 – MODEL SIMULATION

5.1	Introduction	82
5.2	Implementation of the Model Simulation	83
5.2.1	Diaphragm Type	84
5.2.2	Simulation Parameters and MATLAB Programming	87
5.3	Results of the Optical Model Simulation	90
5.4	Summary of the Optical Model Simulation	99

CHAPTER 6 – HARDWARE AND EXPERIMENTAL SETUP

6.1	Introduction	101
6.2	Platform and Moving Target Translational Stage	102
6.3	Actuation Pump	105
6.4	Control Unit and Personal Computer Interface	107
6.4.1	Stepper Motor Control Via Parallel Port Cable	109
6.5	Diaphragm Fluid Lens and Camera Setup	113
6.5.1	Fluid Lens Fabrication and Mounting	113
6.5.2	Diaphragm Fabrication	120

6.5.3	Lighting and Camera Setup	127
6.6	Overall System Integration	129
6.7	Summary	133

CHAPTER 7 – EXPERIMENTS AND RESULTS

7.1	Introduction	134
7.2	Modulation Transfer Function Comparison Study	135
7.3	Focus Measure Development and Testing	145
7.3.1	Optimum ESW Value for a Focused Image	153
7.3.2	Consistency of ESW Measurement	154
7.3.3	Aperture Comparison Result	160
7.4	Hysteresis of Fluid Pump Detection by ESW Value	168
7.5	Auto-Focus Implementation	172
7.5.1	Trend of the Focus Measure	172
7.5.2	Single-Direction Focus Search	174
7.5.3	Dual-Direction Focus Search	178
7.5.4	Auto-Focus Using Focus Measure Error Method	194
7.6	Summary	217

CHAPTER 8 – CONCLUSION AND RECOMMENDATION

8.1	Research Conclusion	219
8.2	Research Recommendation	220
References		221
Appendices		
A	Graphs for the Diaphragm Shape Analysis	224
B	Focal Length Simulation Results	231
C	Focal Length Difference Simulation Results	236
D	Technical Drawings of the Fluid Chamber Parts	241

LIST OF TABLES

	Page
Table 3.1 Rubber material properties for linear elastic model	40
Table 3.2 Deflections at the diaphragm center computed FEA for 2D axisymmetric and shell models	41
Table 3.3 Von Mises stresses at the center of the diaphragm computed by FEA for 2D axisymmetric and shell models	42
Table 3.4 Details of the published study	49
Table 3.5 Lens diaphragm models and their respective parameters	52
Table 5.1 List of parameter values used in the simulation work	87
Table 5.2 The focus pattern across the lens for various diaphragm thicknesses	94
Table 5.3 The focal lengths as measured near the fluid lens diaphragm center for various diaphragm thicknesses at the same applied pressure	94
Table 5.4 Minimum focal length produced by the fluid lens for the various diaphragm thicknesses; noting that the center of the lens is considered for the simulation	95
Table 7.1 Results summary of two focusing operation experiments for two target distances: 265 mm and 865 mm	185
Table 7.2 The average values of the pump motor steps for the two methods, Normal and Error methods. Values of the relative difference of the two methods are tabulated for the respective target distance	204

LIST OF FIGURES

	Page
Fig. 1.1	Research methodology flow chart. 6
Fig. 2.1	Design variations of the fluid lens; A, flexible aperture and hydrogel microposts; B, rigid aperture and hydrogel ring (Dong et. al., 2006) 14
Fig. 2.2	Fluid lens diaphragm cross-sectional view (Kaneko et. al., 1995) 19
Fig. 2.3	Variation in focal length versus volume of fluid (Agarwal et. al., 2004) 21
Fig. 2.4	Microlens doublet operation modes; A, inflated lens forming convex shape; B, deflated lens forming a meniscus (Jeong et. al., 2004) 23
Fig. 2.6	Lens profile across its diameter according to pressure drop between -10 KPa to 10 kPa measured with optical interferometer (Jeong et. al., 2004) 23
Fig. 2.7	The schematic diagram of the actuation mechanism; A, side view of fluid lens; B, servo-motor actuation mechanism (Ren et. al., 2006) 26
Fig. 2.8	Schematic diagram of the actuation mechanism for the liquid pressure variable focus lens system (Kuwnao et. al., 2005) 27
Fig. 2.9	Prototype of the variable focusing microlens chip utilizing heater based actuation method (Wang et. al., 2005) 28
Fig. 3.1	Single-clamped Diaphragm under pressure 31
Fig. 3.2	Outline of the type and method of the FEA study 36

Fig. 3.3	2D axisymmetric modeling where only half of the diaphragm is modeled and y-axis is the axis of symmetry; A) $D_i = 20$ mm; B) $D_i = 10$ mm	37
Fig. 3.4	Shell modeling where the entire diaphragm is modeled; A) $D_i = 20$ mm; B) $D_i = 10$ mm	38
Fig. 3.5	Plotted data for the FEA results of 2D axisymmetric; (A) and (B) graphs of axisymmetric modeling for D20 and D10 diaphragms respectively	43
Fig. 3.6	Plotted data for the FEA results shell models; (A) and (B) graphs of shell modeling for D20 and D10 diaphragms respectively	44
Fig. 3.7	Diaphragm dimensions of the published work	49
Fig. 3.8	Comparison graph between FEA simulation and published measured data of diaphragm fluid lens deflection	50
Fig 3.9	Deflection of the four diaphragm models under applied pressure as simulated by the FEA software: deflection vs. pressure	54
Fig 3.10	Deflection vs. radial position of the diaphragm; (A) and (B) profile plots of the 4 models at 0.5 KPa and 2.5 KPa respectively; (C) profile plot for model 2 at 4.2 KPa	55
Fig. 3.11	overlapped profiles taken at 1.5 KPa pressure for a 50 μ m thick diaphragm	56
Fig. 3.12	Circular fit for the diaphragm profile. Three points are shown through which the circular curve intersects the diaphragm profile for the approximation	58

Fig. 3.13	Plotted results for diaphragm thickness of 100 μm ; (A) deviation from circular profile; (B) coefficient of determination graph	63
Fig 3.14	Diaphragm cross section profile showing the thickness deviation from the original uniform 100 μm thickness diaphragm, under the following pressures; (A) 100 Pa; (C) 3 KPa; (C) KPa 4.2	65
Fig. 3.15	Plotted results for diaphragm thickness of 500 μm ; (A) deviation from circular profile; (B) coefficient of determination graph	66
Fig. 4.1	Lens diagrams and derivation parameters for single-refraction lens	70
Fig. 4.2	Lens diagrams and derivation parameters for double refraction lens	78
Fig. 5.1	Flow chart of the simulation's overall procedure	84
Fig. 5.2	Single-layer diaphragm which represents the top-most layer of the FEA diaphragm	85
Fig. 5.3	Uniform thickness diaphragm which represents two replicates of the top-most layer of the FEA diaphragm, placed at a similar distance as the diaphragm thickness	85
Fig. 5.4	Variable thickness diaphragm which represents actual top and bottom layers of the FEA diaphragm with variable cross-section thickness	86
Fig. 5.5	Various parameters for the diaphragm fluid lens	87
Fig. 5.7	Focal length pattern for a diaphragm fluid lens of 2000 μm thickness; A, 3 kPa; B, 19 kPa	91

Fig. 5.8	Focal length pattern for a diaphragm fluid lens of 250 μm thickness; A, 10 Pa; B, 50 Pa; C, 6 kPa	92
Fig. 5.9	Focal length pattern for a diaphragm fluid lens of 100 μm thickness; A, 100 Pa; B, 3 kPa; C, 4.2 kPa	93
Fig. 5.10	Focal length difference for diaphragm comparisons (thickness = 2000 μm); variable thickness vs. uniform thickness; single layer vs. uniform thickness; A, pressure = 3 kPa; B, pressure = 19 kPa	97
Fig. 5.11	Focal length difference for diaphragm comparisons (thickness = 100 μm); variable thickness vs. uniform thickness; single layer vs. uniform thickness; A, 100 Pa; B, 3 kPa; C, 4.2 kPa	98
Fig. 6.2	Side view of the schematic setup showing the distances between the fluid lens, target start position and target end position	104
Fig. 6.3	An illustrative sketch of the syringe-based pump mechanism used for fluid injection and withdrawal, actuated by a stepper motor	106
Fig. 6.4	A schematic diagram showing the various components of the control unit; power supply, stepper motor drivers, relay switches and computer interface port	108
Fig. 6.5	Parallel port pin diagram for female-type connection	110
Fig. 6.6	Input timing diagram for 1-Pulse mode	111
Fig. 6.7	Input timing diagram for 2-Pulse mode	112
Fig. 6.8	The side view of the diaphragm fluid lens assembly. Also the top and side views of the washer and gasket dimensions are shown	113

Fig. 6.9	Diaphragm wrinkle due to plate bending under clamping pressure; a phenomenon that occurs when the diaphragm material is squeezed at the sides	116
Fig. 6.10	initial lens clamp technique using 4-bolts design.	117
Fig. 6.11	Second lens clamp technique using 8-bolts design.	117
Fig. 6.12	Final lens clamp technique using radially distributed 8-bolts design	118
Fig. 6.13	The inclusion of an O-ring in order to ensure leakage free clamp	119
Fig. 6.14	The usage of a rectangular cross-section washer to provide leakage free clamp and less diaphragm deformation	120
Fig. 6.15	Fluid lens holder and mounting fixture to the xyz-translating stage	121
Fig. 6.16	A diagram showing the components of the inert gas system glove box. The system used in the PDMS material handling for the diaphragm fabrication	122
Fig. 6.17	Diaphragm showing the spacer-mould used for diaphragm fabrication which includes; top part, spacer of specific thickness and bottom part	123
Fig. 6.18	Fluid lens and camera coupling schematic diagram	128
Fig. 6.19	The actual fluid lens and camera coupling used in the experimental setup	129
Fig. 6.20	Operational schematic diagram of the over all system integration	130

Fig. 6.21	Front view of the experimental setup showing the diaphragm fluid lens, camera and syringe-based pump	131
Fig. 6.22	Rear view of the experimental setup showing the diaphragm fluid lens, camera, syringe-based pump, guide rail and target object	132
Fig. 6.23	Close up image of the target object	132
Fig. 7.1	An image of one cycle of the MTF target; (left) image by glass lens, (right) image by fluid lens	137
Fig. 7.2	Scale image by the glass lens	138
Fig. 7.3	Scale image by the fluid lens	138
Fig. 7.4	MTF target image captured by the glass lens	139
Fig. 7.5	MTF target image captured by the fluid lens	139
Fig. 7.6	Pixel intensities along the MTF target captured by the glass lens	140
Fig. 7.7	Pixel intensities along the MTF target captured by the fluid lens	140
Fig. 7.8	Spatial frequency values of the MTF target image captured by both glass and fluid lenses	141
Fig. 7.9	Image modulation values for both glass and fluid lenses versus the spatial frequency values of the MTF target	142
Fig. 7.10	Relative MTF values using the actual experimental data versus the spatial frequencies for both glass and fluid lenses	143
Fig. 7.11	Shows the focus measure using edge slope width across a binary target	145
Fig. 7.12	Shows the focus measure using edge slope width across a binary target	147

Fig. 7.13	A flow chart of the algorithm implemented to find the ESW value. This algorithm is called upon by the main program and returns the ESW value	149
Fig. 7.14	A flow chart of the algorithm implemented to find the slope start pixel (S_s)	150
Fig. 7.15	A flow chart of the algorithm implemented to find the slope end pixel (S_e)	151
Fig. 7.16	Experiment results showing the edge slope width for focused image versus target object distance, where average focus measure value is 11.5 pixels	153
Fig. 7.17	An image of the black and white target captured during exposure to projector lamp only; A, the real image of the target; B, the intensity values, ESW value = 24 pixels highlighted by the two vertical parallel lines	155
Fig. 7.18	An image of the black and white target captured during exposure to projector lamp and reduced ambient lighting; A, the real image of the target; B, the intensity values, ESW value = 29 pixels highlighted by the two vertical parallel lines	156
Fig. 7.19	Graphs showing the slope width variation with repeated image capturing under fixed conditions. Four experiments each at a different target distance: A, 365 mm; B, 565 mm; C, 765 mm; D, 965 mm	159
Fig. 7.20	An image captured by the 5 mm aperture of a target at 215 mm distance, ESW = 20; A, actual image; B, the pixel intensity graph	162

Fig. 7.21	An image captured by the 2 mm aperture of a target at 215 mm distance, ESW value = 11; A, actual image; B, the pixel intensity graph	163
Fig. 7.22	An image captured by the 5 mm aperture of a target at 665 mm distance, ESW value = 19; A, actual image; B, the pixel intensity graph	164
Fig. 7.23	An image captured by the 2 mm aperture of a target at 665 mm distance, ESW value = 11; A, actual image; B, the pixel intensity graph	165
Fig. 7.24	An image captured by the 5 mm aperture of a target at 970 mm distance, ESW value = 19; A, actual image; B, the pixel intensity graph	166
Fig. 7.25	An image captured by the 2 mm aperture of a target at 970 mm distance, ESW value = 11; A, actual image; B, the pixel intensity graph	167
Fig. 7.26	Results for the hysteresis study of the fluid pump motor rotation. Four experiments were conducted where each experiment is at a different target distance; 365 mm, 565 mm, 765 mm and 965 mm	169
Fig. 7.27	The hysteresis effect by pump motor rotation for a target object at 565 mm; A, initial image; B, corresponding ESW graph; C, after actuation of pump motor and returning to the initial image; D, corresponding ESW graph	170

Fig. 7.28	The hysteresis effect by pump motor rotation for a target object at 965 mm; A, initial image; B, corresponding ESW graph; C, after actuation of pump motor and returning to the initial image; D, corresponding ESW graph	171
Fig. 7.29	Trend of ESW values (focus measure graph) for a target placed at 215 mm. Images captured with 2 mm aperture	173
Fig. 7.30	Trend of ESW values (focus measure graph) for a target placed at 265 mm. Images captured with 5 mm aperture	174
Fig. 7.31	A flow chart of the algorithm for the single-direction focus search	177
Fig. 7.32	A flow chart of the algorithm for the dual-direction focus search	180
Fig. 7.33	Focus measure curve for a single focus search trial	181
Fig. 7.34	Example of dual-direction focus search in the vicinity of a focused image for a target at 865 mm; A, the initial image before the start of the search for focus direction; B, its corresponding intensity pixel values and ESW value	182
Fig. 7.35	Example of dual-direction focus search in the vicinity of a focused image for a target at 865 mm; A, the image after fluid withdrawal of 33.3 μl ; B, its corresponding intensity pixel values and ESW value	183
Fig. 7.36	Example of dual-direction focus search in the vicinity of a focused image for a target at 865 mm; A, the image after fluid injection of 33.3 μl ; B, its corresponding intensity pixel values and ESW value	184

- Fig. 7.37 Experiment result for dual direction focus search for a target at 186
265 mm; A, the initial image before the start of the search for
focus direction; B, its corresponding intensity pixel values and
ESW value
- Fig. 7.38 Experiment result for dual direction focus search for a target at 187
265 mm; A, the image after fluid withdrawal of 33.3 μ l; B, its
corresponding intensity pixel values and ESW value
- Fig. 7.39 Experiment result for dual direction focus search for a target at 188
265 mm; A, the image after fluid injection of 33.3 μ l; B, its
corresponding intensity pixel values and ESW value.
- Fig. 7.40 Experiment result for single-direction focus search for a target at 189
265 mm; A, the final focused image; B, its corresponding
intensity pixel values and ESW value
- Fig. 7.41 Experiment result for dual direction focus search for a target at 190
865 mm; A, the initial image before the start of the search for
focus direction; B, its corresponding intensity pixel values and
ESW value
- Fig. 7.42 Experiment result for dual direction focus search for a target at 191
865 mm; A, the image after fluid withdrawal of 33.3 μ l; B, its
corresponding intensity pixel values and ESW value
- Fig. 7.43 Experiment result for dual direction focus search for a target at 192
865 mm; A, the image after fluid injection of 33.3 μ l; B, its
corresponding intensity pixel values and ESW value

Fig. 7.44	Experiment result for single-direction focus search for a target at 865 mm; A, the final focused image; B, its corresponding intensity pixel values and ESW value	193
Fig. 7.45	Graph showing the relationship between fluid withdrawal dosage versus ESW error and its corresponding 2nd order polynomial fitting	196
Fig. 7.48	Flow chart for the focus measure error method algorithm	198
Fig. 7.47	Edge slope width values vs. target distances for before and after the first stage operation (burst of steps)	201
Fig. 7.48	Edge slope width decrement values during the first stage operation (burst of steps) versus target distances	202
Fig. 7.49	Graph showing variation in the extra steps versus initial steps burst for various target distances (365 mm, 565 mm, 765 mm and 965 mm)	203
Fig. 7.50	Graphs showing the comparison results between the error method and the normal method for a target object distance at 365 mm; A, initial steps burst vs. normal method; B, extra steps vs. normal method; C, total steps for error method vs. normal method	206
Fig. 7.51	Graphs showing the comparison results between the error method and the normal method for a target object distance at 565 mm: A, initial steps burst vs. normal method; B, extra steps vs. normal method; C, total steps for error method vs. normal method	207

- Fig. 7.52 Graphs showing the comparison results between the error method 208
and the normal method for a target object distance at 765 mm; A,
initial steps burst vs. normal method; B, extra steps vs. normal
method; C, total steps for error method vs. normal method
- Fig. 7.53 Graphs showing the comparison results between the error method 209
and the normal method for a target object distance at 965 mm; A,
initial steps burst vs. normal method; B, extra steps vs. normal
method; C, total steps for error method vs. normal method
- Fig. 7.54 Summary of the comparison results between the error method 210
and the normal method for four target object distances; 365 mm,
565 mm, 765 mm and 965 mm. Results showing initial steps
burst, extra steps and total steps for error method vs. normal
method
- Fig. 7.55 Auto-focus operation time for low image processing application 211
(without delay) for both normal method versus error method for
four target object distances; 365 mm, 565 mm, 765 mm & 965
mm
- Fig. 7.56 Auto-focus operation time for high image processing application 212
(with 1 sec delay) for both normal method versus error method
for four target object distances; 365 mm, 565 mm, 765 mm & 965
mm

- Fig. 7.57 Actual image captured by the auto-focus operation using the error method at target object distance 365 mm; A, unfocused image; B, after the burst of steps stage; C, final focused image (after extra steps) 213
- Fig. 7.58 Actual image captured by the auto-focus operation using the error method at target object distance 565 mm; A, unfocused image; B, after the burst of steps stage; C, final focused image (after extra steps) 214
- Fig. 7.59 Actual image captured by the auto-focus operation using the error method at target object distance 765 mm; A, unfocused image; B, after the burst of steps stage; C, final focused image (after extra steps) 215
- Fig. 7.60 Actual image captured by the auto-focus operation using the error method at target object distance 965 mm; A, unfocused image; B, after the burst of steps stage; C, final focused image (after extra steps) 216

LIST OF ABBREVIATIONS

2D	2 Dimensional
3D	3 Dimensional
AA	Acrylic Acid
AC	Alternating Current
CCD	Charge-Coupled Device
CCW	Counter Clock Wise
COD	Coefficient of Determination
CW	Clock Wise
DAQ	Data Acquisition
DC	Direct Current
ESW	Edge Slope Width
FEA	Finite Element Analysis
FL	Fluid Lens
FLMi	Fluid Lens image Modulation
GL	Glass Lens
GLMi	Glass Lens image Modulation
I/O	Input/Output
LC	Liquid Crystal
MTF	Modulation Transfer Function
PDMS	Polydimethylsiloxane
PMMA	Polymethylmethacrylate
PZT	Piezoelectric Transducer
VPP	Voltage Peak to Peak

PEMBANGUNAN SISTEM KANTA CECAIR AUTO-MEMFOKUS

ABSTRAK

Kanta-kanta fokus bolehubah cecair semakin bertambah popular dalam banyak aplikasi di mana kanta-kanta kaca merupakan satu-satunya punca sistem optik. Oleh sebab mekanisma baru kanta-kanta cecair tersebut, di mana cecair ialah faktor utama bagi mengubah fokus, penggunaan kanta cecair di dalam sistem memfokus automatik merupakan kajian utama untuk mengesahkan kebolegunaan kanta-kanta cecair dalam operasi-operasi automatik. Maka, kerja yang dilaporkan di dalam tesis ini berkait dengan pembangunan sistem kanta cecair yang menggunakan suap balik imej untuk maklumat memfokus. Suatu algoritma telah dibangunkan untuk mencapai operasi auto-memfokus, melalui pelbagai cara, bagi sasaran binari dalam jarak 1 m. Sistem tersebut terdiri daripada dua motor langkah - satu untuk menggerakkan sasaran dengan menggunakan rel panduan dan yang satu lagi untuk menggerakkan pam dipacu penyuntik yang menyuntik atau mengeluarkan cecair ke dalam (atau ke luar) ruang kanta cecair. Kanta yang digunakan diperbuat daripada polimer 'polydimethylsiloxane (PDMS)' yang mempunyai kebolehlaluan optik yang tinggi. Air suling yang terkandung di dalam kebuk cecair digunakan sebagai bahantara memacu. Kamera CCD monokrom dipasang secara langsung kepada kanta cecair dengan menggunakan tiub pemanjangan untuk merakam imej hidup sasaran binari tersebut. Lebar cerun profil keamatan piksel sepanjang garisan mendatar melintasi sasaran dipilih sebagai nilai ukuran fokus. Operasi auto-memfokus mengubahkan jarak fokus kanta secara tak bergantung untuk mencapai imej fokus berasaskan analisa suapbalik imej. Kajian bandingan MTF menunjukkan bahawa kualiti imej kanta cecair bersamaan dengan kualiti kanta kaca pada frekuensi ruang yang rendah, manakala kanta kaca memaparkan prestasi yang lebih baik pada frekuensi tinggi.

DEVELOPMENT OF AN AUTO-FOCUSING FLUID LENS SYSTEM

ABSTRACT

Variable focal fluid lenses are gaining popularity in many applications where glass lenses were once the only source for optical systems. Due to the new mechanism of the fluid lens, where fluid is the main factor for focus shifting, application of the fluid lens in an automatic focusing system represents an important study for verifying the viability of fluid lenses in automated operations. Therefore, the work undergone in this thesis deals with the development of a fluid lens system that uses image feedback for focusing information. A software algorithm was devised to achieve auto-focus operation, by a number of methods, for binary targets within 1 m distance range. The system comprises two stepper motors – one for moving the target using a guide rail and the other for actuating the syringe-driven pump that injects or withdraws fluid into (or out) of the fluid lens chamber. The lens was made of polydimethylsiloxane (PDMS) polymer which has high optical transmittance. Distilled water, contained in a fluid chamber, was used as the actuating medium. A monochrome CCD camera was directly attached to the fluid lens by an extension tube to capture live images of a binary target. Slope width of pixels intensity profile along a horizontal line across the binary target was chosen as the focus measure value. The auto-focus operation independently varied the lens focal length to arrive at the focused image based on the image feedback analysis. An error-based focusing method was developed that improved the focusing time over the normal focusing method. A comparative modulation transfer function study has shown that the fluid lens image quality resembles that of a glass lens at low spatial frequency whereas glass lens performs better at high spatial frequency.

CHAPTER 1

INTRODUCTION

1.1 Research Background

Lenses have occupied an important role in the advancement of new applications ranging from medical, industrial and communicational areas. Since various applications require different type, design and operation environment of lenses, therefore lenses have become diverse in varieties. In general, lenses are divided into two types: fixed focal length lens and variable focal length lens. The optical quality of fixed focal length lenses was always the benchmark, however such lens is only beneficial for applications where focal length is meant to be fixed and unchanging. Therefore, when an application requires a dynamic optical device where the lens focal length is variable, then fixed focal length lenses are ruled out. Variable focal length lenses, on the other hand, have more complicated structure and produce less optical quality as compared to its counterpart. But, the advantage of having a lens with variable focal length that provides extra functionality and flexibility outweighs some of these difficulties and shortcomings.

Conventionally, variable focal length lens is made up of two or more fixed focal lenses that are placed together along a single optical axis and at least one lens is capable of translation along the optical axis. Therefore, variable focal length is actually achieved by a lens movement in relation with the other lenses. The current optical systems are being hindered by the conventional technology where moving optical elements is done through gears and motors. It has become a major concern to

develop faster and lesser cost technologies. Conventional variable focal length lenses require complicated structures and the inherent contact-friction makes it susceptible to wearing by time and usage, hence becoming less reliable. Moreover, the space required to accommodate the moving parts is large (Ahn and Kim, 1999). Also, producing small and compact optical devices faces manufacturing constraints and high cost (Zhang et al., 2005a). Therefore, new technologies emerged in response to the pressing need and also in an attempt to venture into unexploited potential technologies.

Diaphragm fluid lens is one of the newly developed variable focal length technologies, where the underlying concept is in its deflectable diaphragm. In general, the lens is made of a diaphragm which is bounded to the top of a fluid chamber. The diaphragm curvature changes by changing the fluid volume inside the fluid chamber. Hence, multiple focal planes can be obtained as fluid pressure is varied. Nevertheless, there are challenges related to the development of fluid lenses that need to be addressed. Some of these challenges are with regard to the physical construction of the lens such as diaphragm-thickness effect on optical quality, unsymmetrical deflection of diaphragm, lens size and diaphragm material selection, whereas the other challenges are in terms of operation method such as the dynamical behavior of the lens and auto-focus implementation. As to the awaiting opportunities for variable focus fluid lens system, there are numerous applications such as for in vivo biological imaging (Justis et al., 2004), and adaptive spectacle lenses for vision correction (Douali and Silver, 2004), or for mobile robots vision systems (Bolduc and Levine, 1994), and visual assistance for micromanipulators (Kaneko et al., 1996), or even for surveillance and aerial imaging (Agarwal et al., 2004).

1.2 Problem Statement

Although diaphragm fluid lenses have been the subject of study by many researchers, nonetheless extensive survey showed that the research studies have only dealt with the development of fluid lenses in terms of fabrication, physical features, optical properties and actuation methods. Many studies of fluid lens systems have been reported in the past, such as the work of Ahn and Kim (1999) who used glass diaphragm which is deflected by fluid under static pressure. Kaneko et al. (1998) made a glass diaphragm actuated by PZT bimorph that vibrates at constant frequencies to achieve rapid shifting focal length. Zhang et al. (2005b), Agarwal et al. (2004) and Gunasekaran et al. (2005) used PDMS diaphragm and explored the field of view characteristics of the fluid lens using different lens configurations (telephoto, bi-convex, etc). Justis et al. (2004) used a valveless piezoelectric-pump to inflate the fluid lens diaphragm but with no control to withdraw or hold the fluid from/in the lens. Chronis et al. (2003) made an array of microlenses that is simultaneously pressurized by manual pneumatic regulation. Ren et al. (2006) fabricated a fluid lens chamber with a squeezable reservoir which is cut out around the lens chamber periphery and squeezed by a servomotor-attached string. Few other investigations probed into the effects of diaphragms with built-in convex curvature or non-uniform cross section. It is has been found that the area of auto-focus (closed-loop) control in diaphragm fluid lenses is left open for investigation. Moreover, a holistic approach to the development of a diaphragm fluid lens system is only achieved through the integration in an auto-focus system. Therefore, in this research work the development of a fluid lens with an auto-focus capability was undertaken, where the auto-focus control system uses image-feedback for the control process.

1.3 Research Objective

The main objective of this thesis is to integrate a diaphragm fluid lens into an auto-focusing system with image-feedback control. In addition to the main objective, a few other auxiliary objectives were identified.

- 1) To predict the deflection of different diaphragm thicknesses under applied pressure to determine the design parameters and deflection profiles.
- 2) To examine the deviation of the diaphragm deflection with reference to a circular profile.
- 3) To investigate the fluid lens focal length pattern for a specific diaphragm thickness and compare with other diaphragm thicknesses.
- 4) To design and fabricate a diaphragm fluid lens.
- 5) To develop the hardware and software required for an auto-focus system.
- 6) To devise an algorithm for single and dual direction focus search.
- 7) To optimize the auto-focus operation by focus measure error method.

1.4 Research Scope

The objectives were implemented in view of the following research scope.

- 1) FEA simulation partially represents the true behavior of the diaphragm deflection due to the assumptions of linear material properties, small deflection, uniform diaphragm thickness, symmetrical deflection, etc.
- 2) The theoretical optical study of the fluid lens only takes into account single light frequency into account (i.e. no colors involved).
- 3) The theoretical optical study excludes advanced optical analysis such as aberration, stigmatism and etc.
- 4) Fabricated diaphragm of the fluid lens is assumed to have the same characteristics as reported by published data.
- 5) Fabricated diaphragm thickness assumed to be uniform across the aperture size of the fluid lens due to its small diameter.
- 6) The system hardware runs on a windows-based operating system therefore, no absolute operation time evaluation can be performed.
- 7) The true operation speed of the hardware motors and components is not of relevance to the auto-focusing operation. Rather the relative speed of different auto-focusing operations is the subject of this research.
- 8) The auto-focusing operation shall be system and lens independent. Therefore, the auto-focusing algorithm shall be portable and only images are its controlling factor.
- 9) Due to the above point, many pre-experiment testing and validations are omitted such as fluid lens leakage effect, entrapment of air-bubbles effect, fluid pump dynamics effect, etc.

1.5 Research Methodology

The methodology executed to achieve the outlined objectives is shown in Fig. 1.1.

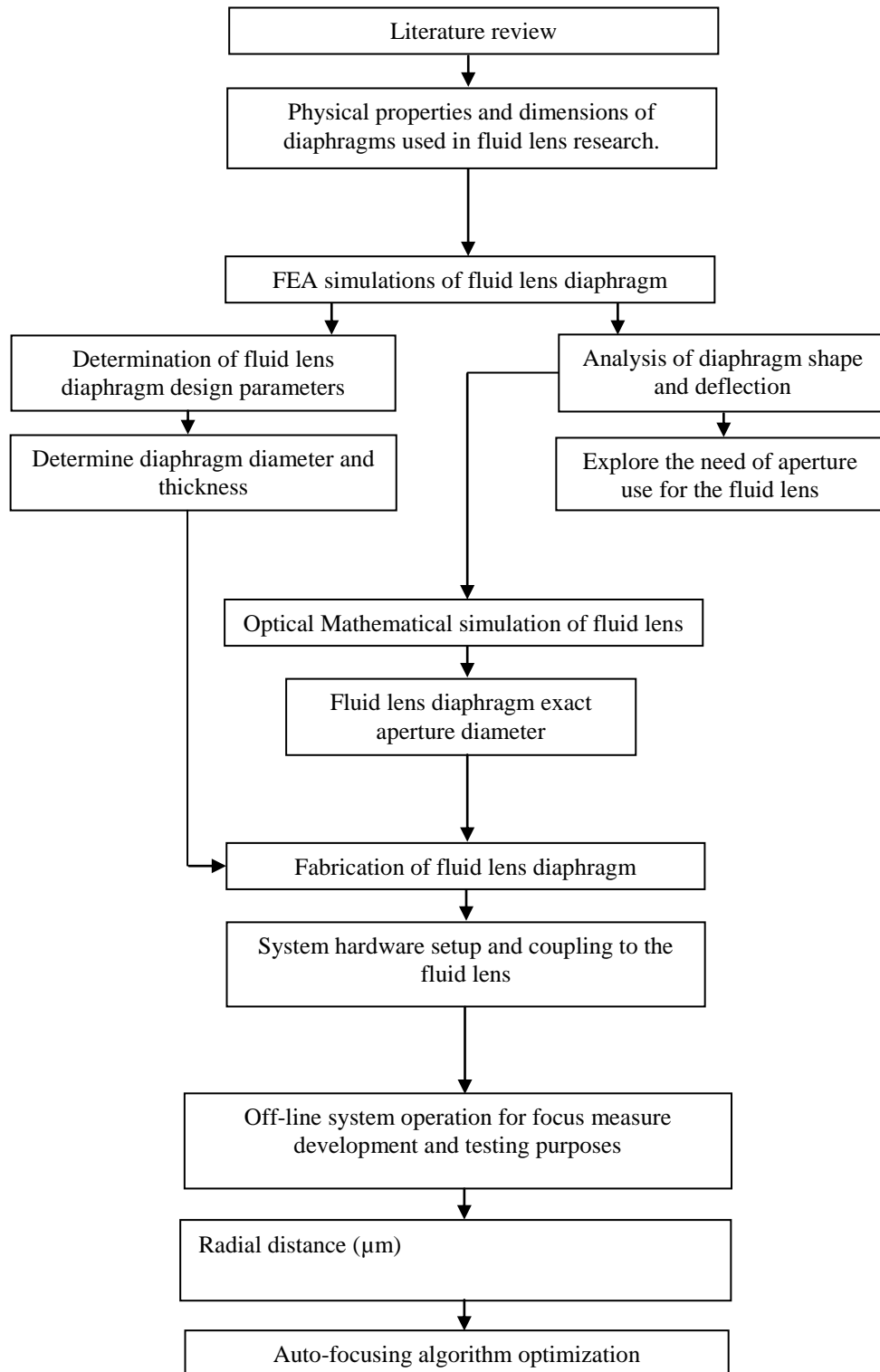


Fig. 1.1 Research methodology flow chart.

1.6 Thesis Organization

The thesis is organized into eight chapters that systematically lead to the objectives of this research. The description of each chapter is as follows:

Chapter 1 gives an introduction to the basics of lens types and points out their drawbacks and advantages. The chapter also presents the concept of fluid lenses. Thereafter, the problem statement of the thesis is elaborated and followed by the research objective. A research scope with a methodology chart is presented for clarity of research flow throughout this thesis.

Chapter 2 presents an extensive literature survey of the past research works on various technologies of variable focal length lenses. The chapter ends with a thorough review of the progress in the control of diaphragm fluid lenses.

Chapter 3 deals with the FEA simulation of the diaphragm fluid lens. A number of analyses performed on the diaphragm behavior under pressure. Also, study of diaphragm deviation from circular profile and thickness variation.

Chapter 4 derives an optical mathematical model that predicts the light rays passing through a fluid lens. Two models are derived, where the first is for a single refraction lens whereas the second is for double refraction lens.

Chapter 5 describes the optical simulation of the diaphragm fluid lens. The simulations were performed by program codes written in MATLAB environment. The chapter takes advantage of the work of the previous two chapters (2 and 3).

Chapter 6 describes the experimental setup, syringe-based pump mechanism and the computer interfacing using the parallel port. Also, the diaphragm fabrication is presented in details along with the fluid lens construction. Finally, the overall system integration is described.

Chapter 7 details the auto-focus experiments and their respective results. The chapter starts with the modulation transfer function comparison between the diaphragm fluid lens and a glass lens. Thereafter, a focus measure is developed, followed by a consistency assessment test for the focus measure. A study on the effects of aperture size is discussed. Finally, the implementation of an auto-focus operation is performed where two methods of operations are devised and tested.

Chapter 8 concludes the work of this thesis and presents potential opportunities for future research work on diaphragm fluid lenses.

CHAPTER 2

LITERATURE REVIEW

2.1 Introduction

New focalizing mechanisms have been the subject of interest in the field of optics. Newly emerging technologies, aimed at the production of variable focal length lenses, such as liquid crystal, hydrogel lenses, electrowetting and diaphragm fluid lenses are presenting various opportunities in the development of lenses, yet requiring more research and implementation strategies. Therefore, in this chapter a review of the few technologies of variable focal lenses is presented thereafter followed by a review on diaphragm fluid lenses where the thesis subject revolves around. This review also introduces the areas where less research has been undertaken with regard to diaphragm fluid lenses as opposed to the intensive research areas carried out by the previous researchers.

2.2 Liquid Crystal Lens

There are currently a number of new technologies that are being adopted for optical applications. Each technology has its own challenges and advantages that make it appealing to some areas of applications. Among these technologies is the liquid crystal technology.

Liquid crystal is commonly used in display applications rather than imaging applications (Knittel et al., 2005). Liquid crystal lenses employ voltage variation in

order to re-orient the liquid crystals resulting in a variation in the index of refraction, in turn resulting in a variable focal length. It is the low voltage and low current requirement that makes liquid crystal based lenses compatible and appealing to digital electronics. However, liquid crystal lenses have a number of design challenges that have to be addressed, such as the time response increases with the square of the cell thickness, also thicker cell structures are harder to maintain. Furthermore, liquid crystal refractive index is crystal-orientation dependent; the smaller the range of angle variation among the crystals, the more uniform is the effective refractive index. Distortion of the electric field across the liquid crystal due to the liquid crystal dielectric interface or by the presence of irregular structure (e.g., Microlens) causes non-uniform index of refraction. Pretilt of liquid crystals, due to variable profile that forms either a convex or concave lens, causes non-constant orientation angle across the lens cell. Therefore, the liquid crystal tilt profile through the cell is not equal.

Commander et al. (2000) introduced the immersion of a microlens array (150 μm in diameter) in liquid crystal material. It was observed that there is a complex optical behavior of the liquid crystal lens due to the effect of photoresist microlens on the liquid crystal structure. As a result, aberration increased in the lens due to two factors: 1), non-uniform electric field due to the presence of the photoresist microlens; and 2), the non-uniform pretilt due to the surface profile of the microlens. The results showed focal length variation from 490 to 1000 μm for 2 to 12 V application, respectively.

Choi et al. (2002) reported a novel method of fabricating an LC microlens (200 μm in diameter) array using a surface relief structure of the UV curable polymer. Their findings showed that microlens profile causes light leakage due to the initial distortion of the liquid crystals along the curved surface.

Knittel et al. (2005) has proposed using convex liquid crystal (CLC) lens in a blue-ray disc optical pickup system in order to compensate for the cover-layer thickness deviation. Liquid crystal material is sandwiched between a glass plate and a plano-concave glass lens to form a convex LC cell. In order to keep the cell thickness as minimum as possible, a very high birefringence LC material of 0.36 was used; therefore, the two sandwich plates had to be separated by only 7 μm . The focal length of the lens is varied by voltage variation from 0 V to 30 V resulting in a 25 cm up to 300 cm focal length. Since, the proposed lens is used in light collimation operation therefore, it has no imaging applications and its focal length exceeds the range within which image-forming applications work.

2.3 Electrowetting-Based Lens

There are other lenses that use liquid-liquid interface as an optical lens. The lens exploits surface-tension characteristics of fluids and the controllability of this characteristic through voltage application is called Electrowetting. Electrowetting-based lenses usually depend on the change of contact of angle of a liquid drop which in turn induces change of its radius of curvature in a liquid-liquid interface, leading to a variable focal length. Such lenses require high voltage applications (75 V and above). In practice, to realize such lens design, two dissimilar refractive index

liquids, yet with the similar densities, have to be used side by side in order to cancel the effect of gravity and to create an interface through which light refracts producing a convex or concave lens. Through voltage application the liquid adhesion to the container wall either reduces (hydrophobic property) or increases (hydrophilic property) causing a change in the liquid surface profile. Due to the restriction of similar density liquids, fewer choices of liquid combinations are available therefore limited number of refractive indices are possible.

Berge and Pescux (2000) proposed the use of external voltage to control the curvature of an Electrowetting-based lens using the technique of gradient wettability. The study dealt with the main characteristics of the lens design such as voltage application, response time improvement by altering liquid viscosity, lens size limit and focal length measurement. For a lens of 5 mm in diameter, the achieved inverse focal length (dioptres) 30 to 100 from 80 V to 200 V, respectively. Although, high voltage was used, it is claimed that the dissipated electrical power is very small such that it is possible to use a very small power supply. The results showed that Electrowetting-based lenses perform best at smaller diameters with no clear limit as to how small it must be.

Hendriks et al. (2005) reported the design and fabrication of a miniature camera employing Electrowetting-based lens. The driving voltage is in the order of 50 - 100 V with response time of 10 ms for full range scan. The lens is 4 mm in diameter with 3 mm inner diameter. A truncated sphere is placed on the top of the lens resulting in a minimum focal length of 20 mm. The results showed good optical quality for image capturing in addition to the viability of focusing at objects lying at

2 cm and 50 cm. however, electrowetting-based lenses come with the requirement of complicated structure design, electrode deposition uniformity, and liquid-type restrictions that contribute to limited potential for various design opportunities.

2.4 Hydrogel-Based Lens

Recently, the concept of forming a lens through liquid-liquid interface was once again adopted but this time with a different actuation method: active hydrogels instead of the previously electrowetting technique. Research was carried in order to integrate such gel capability in altering liquid-liquid interface curvature profile. Hydrogels actively expand and contract upon exposure to a variety of environmental stimuli such as light, electric field, pH, temperature or even antigen. The placement of such hydrogels in a liquid chamber can help produce actuation forces to squeeze the liquid drop or to alter the curvature of a flexible aperture.

Dong et al. (2007) proposed an implementation of a fluid lens that is actuated by using environmentally responsive hydrogels. The fluid lens is made of two chambers placed on each other vertically and separated by an opening (aperture). Each chamber is filled with a liquid of different refractive index. The aperture's bottom surface and inner walls are hydrophilic while the aperture's top surface is hydrophobic. The difference in the aperture surface characteristics is used to maintain a meniscus between liquid/liquid interfaces within a range of high and low pressures. Liquid (water) is pumped into the bottom chamber until its level reaches the top edge of the aperture opening thereafter oil is pumped in the top chamber. The fluid lens was made in two design variations - rigid aperture and ring hydrogel

actuator or flexible aperture and hydrogel microposts, as shown in Fig. 2.1. The lenses are made in diameters ranging from 2 mm to 4 mm and the lenses have tunable focal length from -7.6 mm to $-\infty$ (divergent) and from 8.5 mm to $+\infty$ (convergent).

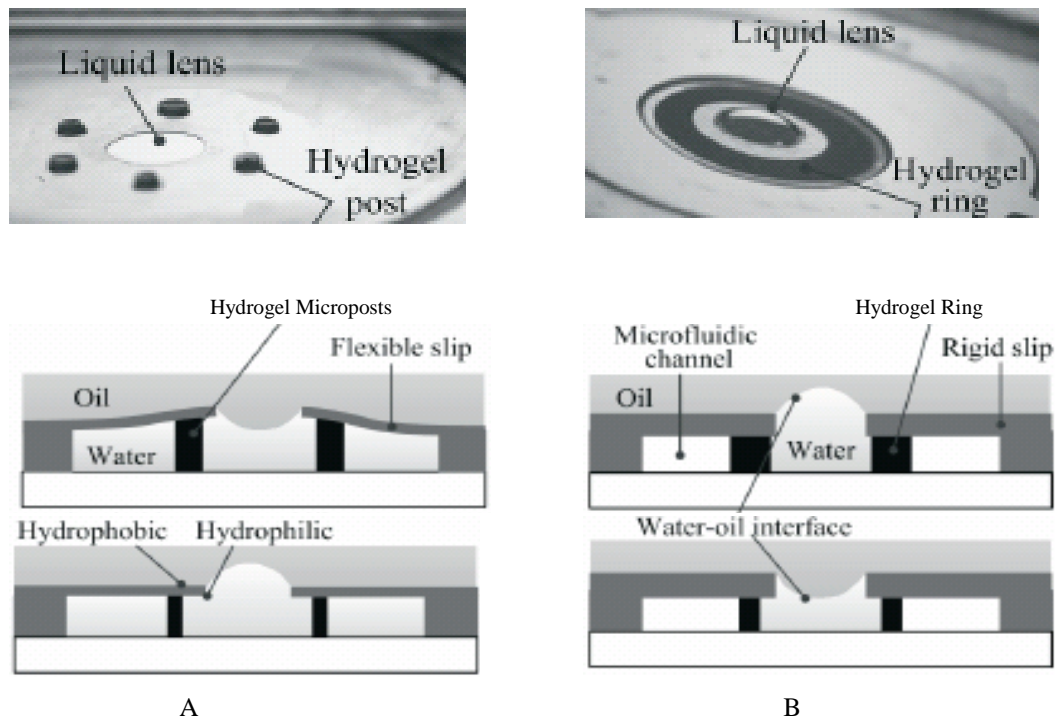


Fig. 2.1 Design variations of the fluid lens; A, flexible aperture and hydrogel microposts; B, rigid aperture and hydrogel ring (Dong et al., 2006a).

Dong et al. (2007) fabricated a rigid aperture with hydrogel ring (as an actuator) sandwiched between the bottom chamber and the underside of the aperture. The hydrogels are either made from Acrylic Acid (AA) pH-responsive hydrogel or N-isopropylacrylamide (NIPAAm) thermo-responsive hydrogel. In pH-responsive hydrogel, various solutions with different pH levels (2 to 12) are passed around the ring surrounding the lens to stimulate it. Since the ring is fixed at the top and the

bottom therefore it expands sideways when it comes in contact with high pH level solution (applying pressure) and contracts when it comes in contact with low pH level solution (reducing pressure). The hydrogel ring is surrounded by polymer jacket that allows the ring to expand only inward and prevents any fluid leakage from above or below the hydrogel ring. As in the case of the thermo-responsive hydrogel, a heater is placed around the lens to heat the hydrogel from 20 °C (maximum expansion) to 50 °C (maximum contraction). In the hydrogel ring design the lens liquid is separated from the stimuli-solution.

In an earlier work, Dong et al. (2006a and 2006b) fabricated a thin flexible aperture with hydrogel micropost actuators erected in the bottom chamber and touching the underside of the aperture. The hydrogels are either made from Acrylic Acid (AA) pH-responsive hydrogel or N-isopropylacrylamide (NIPAAm) thermo-responsive hydrogel. After exposure to variation in either pH level or temperature the microposts expand vertically in the contrary to the case seen by the ring hydrogel (lateral expansion). This is because of the flexible aperture and the microposts are slender which gives them greater vertical than lateral expansion. The change in microposts volume does not alter the fluid pressure directly but rather displaces the flexible aperture vertically which induces change in the meniscus curvature. In the hydrogel microposts design the same stimuli-solution that passes through the hydrogel microposts is used as the lens liquid.

The advantages of the newly proposed hydrogel-based fluid lens lies in the self-sensing and self-actuating hydrogel which forms a closed loop feedback of the lens and requires no power supply for operation. Hence, reducing the complexity of fluid lens system, however stimuli-responsive hydrogels have the slowest response time which is in the order of 10 seconds in comparison to other fluid lenses (electrowetting lens and liquid crystal lens). Moreover, the lens can only operate in self-generated closed loop feedback in stimuli-sensing applications where a detection of environmental parameter variation triggers the actuation or else the lens requires an external support and mechanism to trigger the actuation as the other variable lenses require as well.

2.5 Diaphragm Fluid Lens

Diaphragm fluid lens's structure only requires a liquid chamber that is sealed by a flexible diaphragm which is subjected to fluidic pressure to form convex or concave profiles, hence forming converging or diverging lens, respectively. The only control parameter for producing focal shift in the diaphragm fluid lens is the liquid pressure or volume. Notably, both can be controlled by a variety of means such as electrical, magnetic, mechanical or even pneumatic actuation. Whereas in the case of the other lenses discussed earlier, the actuation method is restricted to either voltage or liquid, such as in electrowetting lenses where hydrophilic and hydrophobic property of the liquid-surface can only be altered by voltage. The same can be said for the re-orientation of the liquid crystals which can only be done through voltage variation.

2.5.1 Lens Theorization, Fabrication, Characterization and Testing

Early work, dating back to 1940, on such lenses was hindered by the lack of suitable flexible diaphragms with good optical qualities. However, first publications dealt with the theorization of the lens deflection and focus shift, such as the work of Sugiura and Morita (1993) who showed theoretically that a fluid filled lens placed horizontally takes on a parabolic shape and approximately a spherical shape at the central area. The authors, for the first time, have investigated the effect of gravity on the fluid lens diaphragm in a vertical orientation and a dimensionless parameter ' k ' was therefore developed to characterize any deformation due to gravity. A theoretical model was derived for the diaphragm deflection which is a function of few variables; fluid pressure, fluid density, lens base radius, gravity constant and diaphragm tension. They reported that diaphragm deformation due to gravity is independent of the diaphragm elastic tension. Experimental images were captured and showed reduction in image distortion due to gravity deformation as the k value increased from 1 to 30, at and above which gravity effect becomes negligible. Nevertheless, k value is not a parameter that can be tuned for each focal length but rather it is the characteristic of each specific focal length. For example, in their experimental result a focal length of 400 mm is characterized by $k = 30$. Therefore, k value could be useful design parameter only if diaphragm type is fixed whereas different fluid densities and lens base radii are to be determined.

Rawicz and Mikhailenko (1996) completed the derivation of the mathematical model for the diaphragm deflection for a horizontally oriented fluid lens by Sugiura and Morita (1993). In the previous work the mathematical model did

not consider the diaphragm tension. In this paper the authors presented an equation for finding diaphragm tension which is a function of Poisson's ratio, diaphragm thickness, fluid pressure and lens base radius. Hence, given the aforementioned properties are known the deflection of a horizontally oriented fluid lens can be calculated. Ray tracing technique was programmed in MATLAB to perform theoretical focal length estimation on the fluid lens. Theoretical and experimental comparisons for focal length were made and both results were in agreement.

Early work such as the aforementioned examined mostly the theoretical modeling and analysis of diaphragm deflection while others have tried to investigate non-uniform diaphragm thickness in order to improve deflection properties and to improve the optical quality and to overcome aberrations. Kaneko et al. (1995) reported an attempt to solve the problem of high aberration at short focal length caused by aspherical deflection of the uniform thickness diaphragm. The author fabricated a glass diaphragm of 11 μm average thickness with a specific thickness profile. According to the findings, uniform thickness diaphragms often deviates from a spherical shape, that is when the diaphragm is deflected by pressurized fluid. Therefore a special thickness diaphragm that can be deflected spherically as shown in Fig. 2.2 was suggested to solve the problem. Finite element analysis was used to calculate the required thickness profile for a specific focal length range beyond which the diaphragm starts deviating from spherical deflection to aspherical deflection. The specific thickness diaphragm has shown improvement from uniform thickness diaphragm. However, the design only resolves the aspherical deformation at a specific focal range (200 mm – 600 mm) while the aspherical deformation throughout the entire focal range is still unresolved. However, attempts are on going

to produce non-uniform diaphragm thickness to reduce aberration and to improve optical characteristics. Zhang and Lo (2003) made a simulation to predict the improvement in diffraction Intensity Spread Function of a uniform versus non-uniform lens diaphragm.

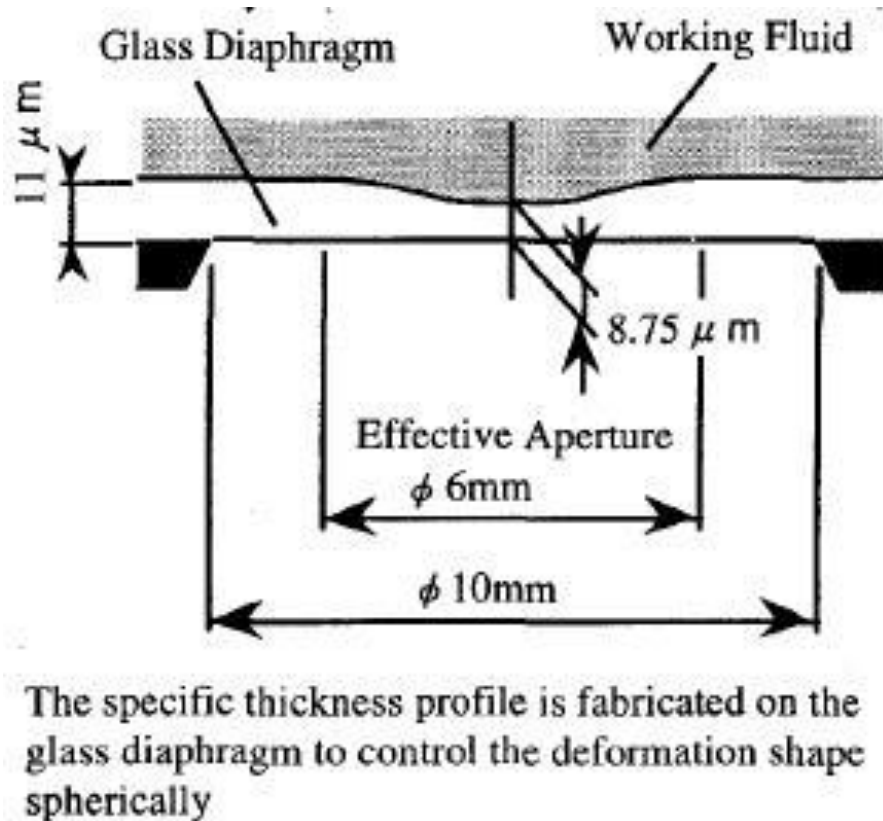


Fig. 2.2 Fluid lens diaphragm cross-sectional view (Kaneko et al., 1995).

Ahn and Kim (1999) on the other hand fabricated a square lens glass diaphragm of 10 mm side length and 40 μm thickness filled with silicon oil ($n = 1.65$). There is high aberration for the square diaphragm due to its square boundary conditions and hence cushion-like deflection. The aberration was calculated

theoretically by the diaphragm curvature. Static pressure was applied to the glass diaphragm to vary the focal length. The numerical aperture of the lens is very small due to the planar glass diaphragm. No images were captured by the lens for verifying the optical quality.

More recent research has explored the use of polymers (polydimethylsiloxane, PDMS) for making the diaphragm. PDMS is favored for its many advantages such as bio-compatibility, high elasticity and good optical transmittance. Zhang and Lo (2003) used polydimethylsiloxane (PDMS) diaphragm lens and mainly experimented with different lens types (convex-concave, telephoto, reverse telephoto, concave-concave, etc) in order to get the largest field of view, numerical aperture and zooming ratio. However, the images captured by their optical system are the images of light-emitting diodes (LED) therefore no conclusive results were obtained with regard to image distortion and the lens's optical quality.

Research into maximizing the field of view was carried out further by Gunasekaran et al. (2005) with a fluid lens of 15.8 mm diameter and 1.5 mm chamber depth. The chamber was covered on both sides by the PDMS diaphragm to form either biconvex or biconcave lenses. Single and multiple fluid lenses were used in combinations to produce a large field of view and the experiments were verified with real life images. Distortion was apparent in the experiment images, whereby as the field of view increases (i.e., focal length decreases) the distortion increases too. The maximum field of view achieved is 118.3° through one camera glass biconvex lens and three biconcave fluid lenses. A single biconvex fluid lens was able to be

tuned to achieve a minimum of 20.54 mm focal length. The membrane pressure for all the lenses was statically varied by means of manual operation.

Agarwal et al. (2004) fabricated 4 mm diameter lens using PDMS. The lens can be formed into either biconvex or biconcave as well. A similar investigation to Gunasekaran et al (2005) was made, with the exception that this lens is smaller in size and only a single biconvex or biconcave fluid lens was used in conjunction with the camera glass lens to maximize field of view. It was observed that the field of view for the biconvex and biconcave lenses can be tuned in the range of 0.12 to 61° and 7 to 69°, respectively. The nonlinear relationship between the focal length and the fluid volume in the fluid lens was plotted as in Fig. 2.3. The nonlinearity implies that at long focal length the lens is sensitive to small volume changes and at short focal length the lens is comparatively less sensitive to small volume changes

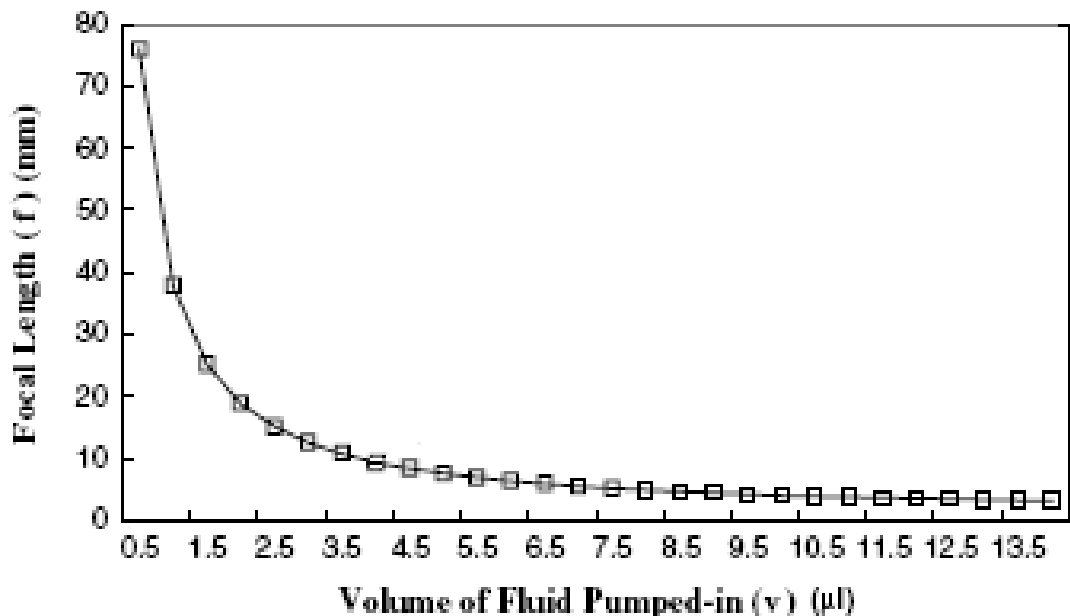


Fig. 2.3 Variation in focal length versus volume of fluid (Agarwal et al., 2004).

Chronis et al. (2003) fabricated an array of microlenses made of PDMS. The microlens array is simultaneously pressurized by means of manual pneumatic regulation. The lens is made of PDMS diaphragm (200 μm in diameter and 40 μm thick). When microscope immersion oil ($n = 1.51$) was used as filling liquid, the PDMS lens diaphragm reacts with the filling liquid and exhibited swelling. White light interferometer method was used to inspect the diaphragm profile but only after coating the lens diaphragm with a thin gold layer.

Chen et al. (2004) fabricated a PDMS diaphragm with a 3D convex shape which was then placed on a microfluidic chamber to form the fluid lens. The 3D convex micro lens provides a focal point even at the initial position unlike the other fluid lenses. The lens's diameter is 1.4 mm and 85 μm is the height of the convex diaphragm. It was reported that the built-in convex shape provides much higher numerical aperture (0.24) than a planar glass or polymeric diaphragm. However, image quality improvement for this design was not reported.

Jeong et al. (2004) reported a tunable microdoublet lens made entirely of polydimethylsiloxane (PDMS) with diameters of 300 μm to 500 μm . The reported design differs from previously reported microsinglet lenses because it can operate in both biconvex or meniscus modes. This is achieved by molding the bottom of the fluid chamber into a fixed negative microlens that is capped by a thin membrane which forms the variable curvature surface, as shown in Fig. 2.4. Manual pneumatic pressure application from -10 kPa to 10 kPa produces deflection in the range of -7.5 μm to 6 μm , respectively as shown in Fig. 2.5.

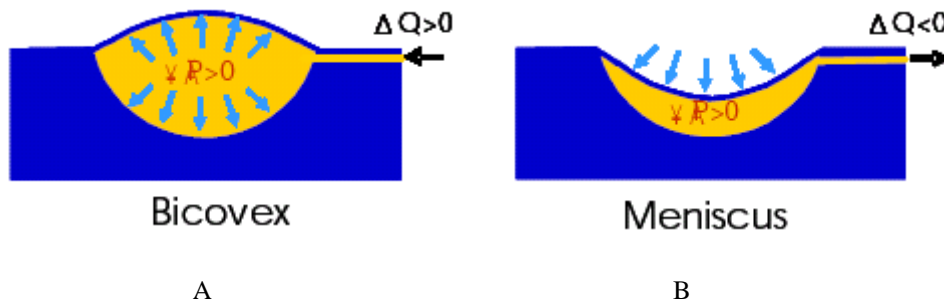


Fig. 2.4 Microlens doublet operation modes; A, inflated lens forming biconvex shape; B, deflated lens forming a meniscus (Jeong et al., 2004).

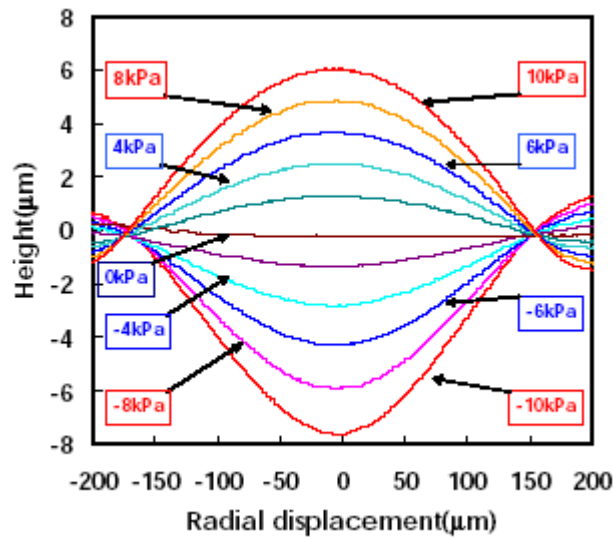


Fig. 2.5 Lens profile across its diameter according to pressure drop between -10 kPa to 10 kPa measured with optical interferometer (Jeong et al., 2004).

Werber et al. (2005) fabricated an array of nine microfluidic lenses of 400 μm diameter each. The microlenses were fabricated from PDMS diaphragm spun on an Si wafer. Manual pressure control was implemented to vary the pressure from 0 kPa to 54 kPa and it was noted that maintaining constant pressure is important to prevent variations in the focal length during the imaging period. Also, no hysteresis observed in membrane deflection especially with low maximum pressure values although extremely high pressures may overstretch the PDMS membrane causing plastic deformation. Also it was noticed that the fixed edge of the membrane leads to an inflection point at the lens edge (Fig. 2.6). The inflection point produces concave

curvature at positive pressure instead of convex as would be the case for a completely spherical lens but an additional aperture can minimize the aberrations that are due to the lens edge.

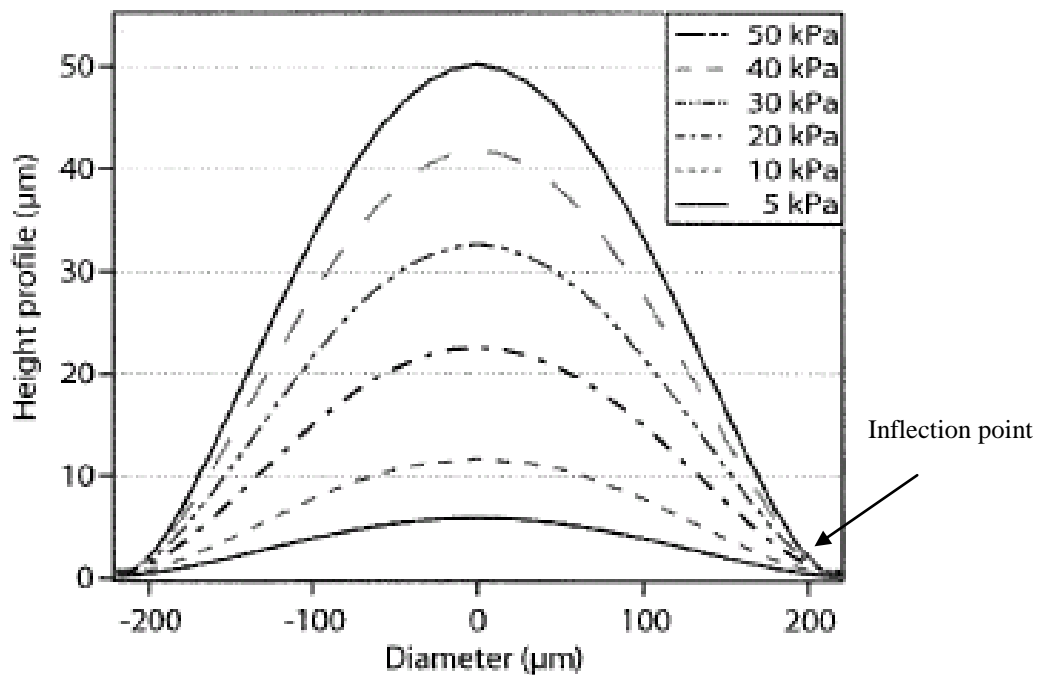


Fig. 2.6 Lens profile as predicted by ANSYS simulation (Werber et al., 2005).

2.5.2 Actuation Methods and Control

So far the research was mainly concerned with the physical characteristics and analysis of the fluid lens itself. Nonetheless, work on the actuation methods for diaphragm fluid lenses has also progressed. An early actuation scheme proposed by Kaneko et al. (1998) where a fluid lens made of glass diaphragms with integrated piezoelectric bimorph actuators for diaphragm push/pull action was developed. The